Cytometry Part A 71A:80–86 (2007)

Original Article

# Automated Laser Scanning Cytometry: A Powerful Tool for Multi-Parameter Analysis of Drug-Induced Apoptosis

**Andrea Lisa Holme,[1] Sanjiv Kumar Yadav,[2] and Shazib Pervaiz[1–3]***

[1]ROS Biology and Apoptosis Group, National University Medical Institutes
[2]Department of Physiology, Yong Loo Lin School of Medicine
[3]NUS Graduate School of Integrative Sciences and Engineering, National University of Singapore, Singapore

Received and Accepted 27 November 2006

**Background:** Simultaneous analysis of multiple intracellular events is critical for assessing the effect of biological response modifiers, including the efficacy of chemotherapy. Here we used the automated laser scanning cytometry (LSC) for multi-parameter analysis of drug-induced tumor cell apoptosis.

**Materials:** Using 2-mercaptopyridine-*N*-oxide-hydrate sodium salt, or the commonly used chemotherapeutic agents etoposide and camptothecin, we performed simultaneous analyses of apoptosis-related morphological features as well as fluorescence-based biochemical changes in a 96-well format.

**Results:** We demonstrate the scope of LSC as a platform for comparing multiple variables between different cell populations, distinguishing unique events at a single cell level within a sample population, and enabling simultaneous screenings in a single assay at multiple dosages and time-points.

**Conclusion:** These data underscore the power of LSC for simultaneous multi-parameter analysis, which could have implications for screening or assessing the efficacy of drug responses in heterogeneous cell populations and at the single cell level. © 2007 International Society for Analytical Cytology

**Key terms:** laser scanning cytometry; apoptosis; mitochondria; multi-parameter; 2-mercaptopyridine-*N*-oxide-hydrate sodium salt; cancer cells

Conventional flow cytometry (FCM) allows assessment of single biochemical or molecular parameter, and therefore, cells manifesting atypical feature(s) or phenotype(s) usually escape analysis (1,2). This is a major drawback when classification of phenotypical changes is based on multi-parameter changes at the single cell level or in a heterogeneous population of cells. For instance, a complete assessment of the mode of cell death requires a multitude of parameters, morphological as well as biochemical, to be analyzed over a period of time (3–5). Conventional methods only allow for examination of multiple samples in separate assays on an individual basis and fall short of providing a simultaneous assessment of morphological and biochemical events. The advent of amalgamable dyes, sophisticated FRET based assays for protein functions/interactions, and genetic tagging systems, has opened up the field of multi-parameter analysis, rapidly expanding our understanding of cellular events and pushing the boundaries of analytical technology (6–8). In line with these advances, concerted efforts to consolidate the advantages of flow and image cytometry have given rise to slide-based Laser Scanning Cytometry (LSC). The LSC addresses areas in which the fluid based cytometry is deficient; solid phase preparations, attached adherent cell lines, tissue sections and arrays, cytological smears, small clinical needle biopsy samples and FISH, can all be easily analyzed, while preserving the capacity to analyze fluid specimens (9,10). The LSC measures laser light scatter and absorption with fluorescence emissions, and uses laser light scatter in a bright-field visualization mode to give both quantitative and qualitative data (11). Moreover,

Part of this manuscript was presented at the 11th Leipziger Workshop, April 27–29, 2006, BioCity Leipzig, Germany, www.leipziger-workshop.de

Grant sponsors: The National Medical Research Council and the Biomedical Research Council Singapore; The Academic Research Fund, NUS, Singapore.

*Correspondence to: Shazib Pervaiz, M.D., Ph.D., Department of Physiology, NUS Graduate School of Integrative Sciences and Engineering, Yong Loo Lin School of Medicine, National University of Singapore, 2 Medical Drive, MD9 No. 03-06, Singapore 117597.

E-mail: phssp@nus.edu.sg

Published online 2 January 2007 in Wiley InterScience (www.interscience.wiley.com).

DOI: 10.1002/cyto.a.20362

samples are preserved along with the coordinates of their position on the platform, thereby allowing precise relocation of a specific cell/event for further evaluation.

Over the past couple of decades, the mechanisms by which cells' undergo death have been intensely scrutinized using a barrage of approaches to examine the effects of stimuli on growth, survival, and death pathways. Many of the available techniques address the characteristic changes that occur such as: morphological changes, metabolic changes like oxidative stress and intracellular pH, ionic fluxes, mitochondrial morphology and function, and DNA integrity, to furnish an understanding of the complexity and diversity of the processes involved in cell survival and maintenance of tissue homeostasis. These sets of variables have allowed scientists to classify cell death modes into apoptosis and programmed cell death, necrosis or accidental cell death, autophagy, and other hitherto unclassified death phenotypes. Apoptosis is a genetically preordained cell death orchestrated by intracellular caspases (caspase 1–14) and involves an intricate crosstalk between caspases, intracellular organelles, such as mitochondria, lysosomes, endoplasmic reticulum and nucleus, and the Bcl-2 family. In sharp contrast, necrosis is viewed as an uncontrolled cell death process, involving the release of cellular products into the extracellular environment, and eliciting a strong inflammatory response. Indeed, it was from the premise of the divergent morphological features used by pathologists to distinguish between enzymatic digestion and/or protein denaturation cell death, that the famous article of Wyllie and coworkers came about, in which apoptosis and necrosis were first characterized (12). Since their pioneering work, morphological changes, more or less, have served as the gold standard for determining the mode of cell death. And therefore, flow-based assays have routinely been used to monitor cell size/volume, DNA hypoploidy, organelle-specific changes, protease activation, cell surface receptor expression, etc., to study cellular response to physiological as well as pathological stimuli (13–16). Although, powerful and highly informative, flow-based analyses carry an inherent problem of missing out on actual imaging of events as well as simultaneous evaluation of multiple parameters. This has been circumvented by the advent of newer platforms, such as the LSC, which enables simultaneous evaluation of multiple biochemical, molecular and cytometric markers, in combination with morphological analysis of single cells within a whole population, and the subsequent correlation of ongoing intracellular events with cellular response(s) (9,17). In addition, these assays could be performed in a variety of formats, such as slide-based and multi-well plate. On the backdrop of this, we have utilized the LSC (CompuCyte) with the iCys platform technology equipped with 3 lasers; Violet 405 nm, Argon 488 nm, and Helium/Neon 633 nm, and the filter cube sets 463/39, 530/30, 580/30, and 630/LP, coupled with the iCys confocal module for in-depth investigation of cellular events during drug-induced apoptosis. Using the adherent Chinese Hamster Ovarian (CHO) cell line, we investigated the effect of 2-mercaptopyridin-*N*-oxide-hydrate sodium salt (MPO-Na) on a number of parameters consistent with apoptosis, such as cell segmentation, cell cycle, DNA content and damage, mitochondrial transmembrane potential, plasma membrane integrity as well as cellular morphology to obtain both quantifying and qualifying data pertaining to cell death signaling.

## ACQUISITION AND ANALYSIS OF DATA USING LSC

When obtaining data, the scan data was first segmented to associate specific pixels with each event data from a selected channel and used to draw a contour around all of the adjacent pixels above a preset threshold value (set by the user to define an event). In addition to analyzing the integrated fluorescence (integral) of a cell, the LSC can collect the fluorescence data for individual pixels within a cell area, and express this as fluorescence signal (max pixel). The data could be displayed as histograms or scatter plots, and scan-field images, together with the statistical analysis for a given sample (one well). Furthermore, a group of wells or a scan area may be defined by regions to obtain specific data from this group, and groups may be displayed as averages and color-coded according to expression or density.

## GROSS DETERMINATION OF CELLS UNDERGOING APOPTOSIS

### Cell Segmentation and Cell Cycle Analyses

The ability of the LSC to count live cells while affixed to their growth surface has allowed us to extrapolate this ability to determine both the cell number and the formation of cell clusters/single cell segmentation. This feature is important when determining the usefulness of a potential chemotherapeutic agent. As shown in Figure 1a, using the cell permeable dsDNA nuclear dye Hoechst 33342, a two-fold serial dilution of MPO-Na [83.8 μM (high) to 0.327 μM (low)] resulted in prominent cell segmentation over increasing dosages, which could be an indication of inhibition of tumor colony formation. The observation that cell clusters became segmented single cells upon drug treatment is measurable using the LSC's contouring feature, where the user defines a set value for the size and threshold, thus allowing the ability to distinguish between single cells and clusters of cells based on their size and on the fluorescent intensity. Furthermore, when compared with the standard chemotherapeutic drugs, camptothecin (dose range 1.5 μM to 2.9 nM) and etoposide (dose range 12.5 μM to 24 nM), MPO-Na was more effective in inducing single cell segmentation, which provided the impetus for the assessment of its anti-cancer potential. Figure 1b shows that for the same samples from Figure 1a we were able to reanalyze the cell cycle profile and readily obtain histograms of the DNA profile (blue integral). These data clearly demonstrate that treatment of cells with MPO-Na resulted in a significant increase in the G1 fraction of cells at moderate to high concentrations, thus indicating G1 cell cycle arrest. Moreover, subjecting these data to statistical scrutiny using the D-value Kolmogorov–Smirnov analysis (KS) verified statistical significant difference in the effect of MPO-Na with increasing concen-

tration, which corresponded to a change in the cell cycle profile (Fig. 1c).

### Nuclear Changes

Changes to the nucleus are considered hallmark features of apoptosis and are characterized by the processes of karyolysis, karyorrhexis, and pyknosis. When DNA analysis in living cells is undertaken, the purpose is often the determination of DNA content, cell cycle profile, and the amount of DNA damage induced by the agent (18). Investigation of the DNA content could be performed with dyes such as propidium Iodide (PI) and Hoechst 33342 that readily intercalate into nucleic acids, while a reliable marker for the induction of double-stranded DNA breaks is histone H2AX phosphorylation on $Ser^{139}$ (γH2AX) (17,19–21). Here we demonstrate the strength of the LSC in providing a simultaneous bi-variant analysis of DNA content as well as DNA strand breaks using different fluorophores. Figure 1d shows a density plot of the γH2AX staining (green integral) against the DNA content (crimson integral). At lower concentrations, MPO-Na caused two main populations designated as R1 (negative for γH2AX staining and colored coded red) and R2 (γH2AX positive and color coded green). Any cells above these regions are live cells, while the cells below are apoptotic bodies and cellular debris. At higher concentrations, the majority of the cells are lost, thus illustrating a technical difficulty when analyzing highly apoptotic populations by indirect immunofluorescence.

To obtain further insight into the morphological changes associated with drug exposure, we made use of the newly developed live-cell confocal imaging feature of the LSC, which allows simultaneous live cell imaging with other biochemical parameters. Figure 1e shows the images of cells with MPO-Na stained with the cell permeable dyes SYTO16 Green (for all nucleic acids) and Hoechst 33342 (dsDNA). A hitherto unexplained feature of large dark "holes" or hollowing of the nucleus, undetected with the LSC's normal fluorescence microscope, was observed in drug-treated cells.

### Morphological Analysis

In tissue culture systems, a good starting point for the analysis of apoptosis is the use of the microscope. The customary sequence of morphological changes are; (1) loss of adhesion to the substratum resulting in cell rounding, (2) a flurry of surface zeiotic blebbing, (3) shrinkage of the cell with the cessation of blebbing and other movements, (4) in some cells the formation of protrusions of elongated "echinoid spokes" from the cell surface and (5) after a delay, the blistering of the cell surface membrane which eventual undergoes lysis similar to necrosis (22–24). Utilizing the LSC's imaging capability MPO-Na treatment was observed to induce dramatic morphological changes consistent with apoptosis, including cell rounding and loss of attachment (anoikis), as shown in the field scan images in Figures 1a and 2c.

### Plasma Membrane Permeability

Cell membrane permeability is usually assessed by the ability of cells to readily take up fluorescent dyes, a common feature associated with a variety of cell death phenotypes. The most widely used dyes for this purpose are those that label nucleic acids e.g., Propidium Iodine (PI) and YO-PRO-1. The cell membrane impermeable YO-PRO-1 (629 Da) is a popular dye, reported to enter via the P2X7 ion gated channel, which becomes (more) active concurrently as phosphatidylserine (PS) is externalized, thereby allowing the monitoring of apoptotic phases (25,26). However caution is perhaps warranted, as although this assay provides a means for distinguishing early apoptotic cells from late apoptotic/necrotic cells, it is in fact little more than a measurement of membrane channel integrity. The sample population from Figure 1a was used for further investigation by adding the dye combination of YO-PRO-1 (green for early apoptotic cells), PI (red for late apoptotic cells), to the Hoechst 33342 (blue for double stranded DNA) treated cells. In the Cartesian plate map in Figure 2a each block of pixels represents a well color-coded according to the density of YO-PRO-1 uptake, and shows that only cells treated with MPO-Na stained for YO-PRO-1, and that apoptotic cells were primarily located in the wells with the highest concentrations of the compound. A further analysis of the scattergrams of selected wells shows that as the dosage of MPO-Na increased there was a shift in the cell population from R5 to R3 to R2 i.e., from the right to the left of the scatter plot (Fig. 2b), indicating that YO-PRO-1 staining decreased with a reciprocal increase in the fraction of cells with small condensed DNA as the integral value decreased. In Figure 2c bright field analysis shows that there was a concordant decrease in cell size, and the loss of YO-PRO-1 signal could be attributed to dye leakage from cells undergoing late apoptosis.

FIG. 1. Exposure of CHO cells to MPO-Na reduces tumor cell clusters and increases segmented single cells, induces a G1 cell cycle block, together with double-strand breaks. Cells were treated with increasing concentration of drugs [MPO-Na (0.327–83.8 μM), camptothecin (2.9 nM–1.5 μM) or Etopside (24.4 nM–12.5 μM)] for 24 h before being stained with Hoechst 33342 (10 μg/ml; incubated for 30 min at 37°C) and scanned using the LSC. (**a**) Data are plotted as single cell segmentation against wells of increasing drug concentrations; (**b**) Multi-well analysis of cell cycle profile of MPO-Na treated cells from (a) were done using Hoechst 33342; (**c**) Cell cycle Kolmogorov-Smirnov (KS D-value) histograms are shown for the same data set showing differences between the treated and untreated cells; (**d**) Scattergrams of the samples were obtained using the crimson channel to identify the PI (DNA) staining. γH2A was detected on the green channel for the Alex Fluo 488; cells where treated as described in Figure 1a, fixed in ethanol for 30 min at 25°C, blocked with 1% BSA in PBS before incubating for 1 h with the polyclonal phosphorylated histone H2AX antibody (Trevigen, 1:100), and Alexa 488 goat anti-rabbit (Molecular Probes, 1:200) as secondary antibody. Cells were counterstained by adding 5 μg/ml of PI and 200 μg/ml RNAase in PBS and incubated in the dark for 30 min; (**e**) cells where treated with MPO-Na for 24 h before being stained with Hoechst 33342 (bright staining) and SytoGreen16 (diffused pattern) and visualized with LSC's confocal platform. Arrows indicate prominent vacuoles, seen in the nucleus of MPO-Na treated CHO cells.

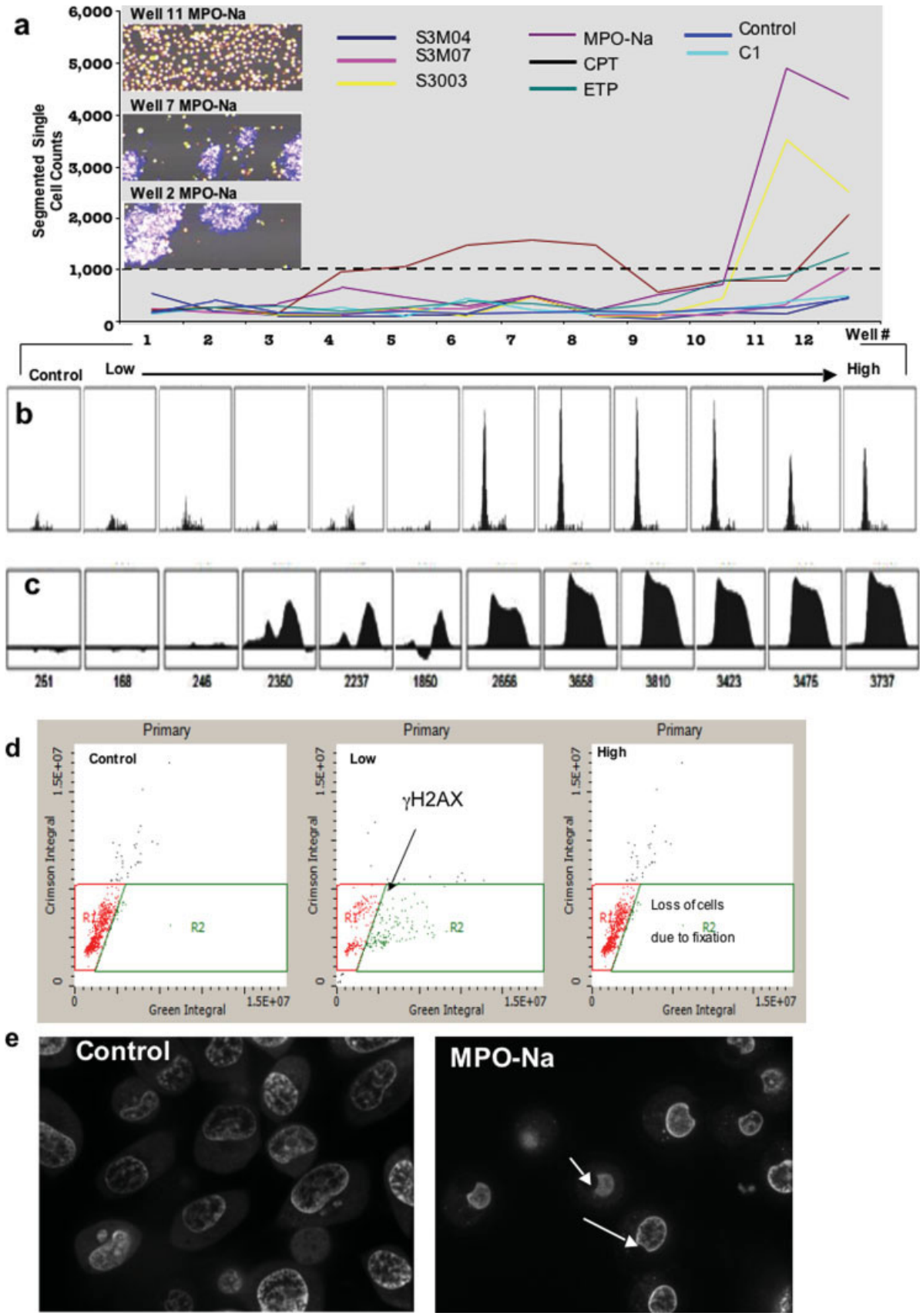
a
Well 11 MPO-Na
Well 7 MPO-Na
Well 2 MPO-Na
S3M04
S3M07
S3003
MPO-Na
CPT
ETP
Control
C1
Segmented Single Cell Counts
6,000
5,000
4,000
3,000
2,000
1,000
0
1 2 3 4 5 6 7 8 9 10 11 12
Well #
Control
Low
High
b
c
251 168 246 2360 2237 1850 2656 3658 3810 3423 3475 3737
d
Primary
Control
Low
High
γH2AX
Crimson Integral
Green Integral
1.5E+07
R1
R2
Loss of cells
due to fixation
e
Control
MPO-Na

FIG. 1.

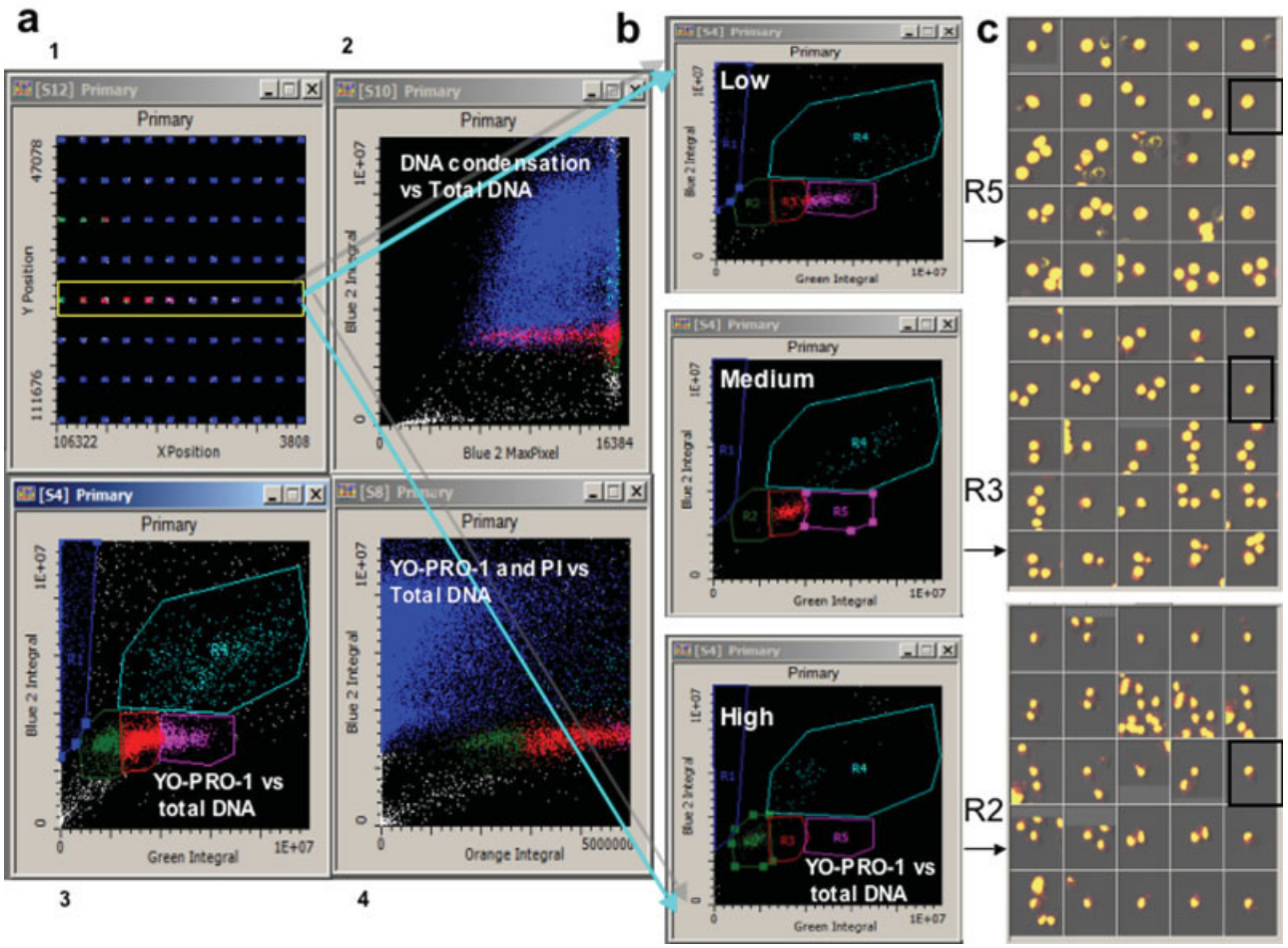


FIG. 2. Cartesian Plate Map of Cells Stained with YO-PRO-1 versus Hoechst 33342. Cells are treated with the titrated drug range (indicated by the yellow box) for 24 h before being stained with Hoechst 33342 (10 μg/ml), and YO-PRO-1 (10 μg/ml), PI (1 μg/ml) and incubated at 37°C for 30 min. (**a**1) All the wells are compared for YO-PRO-1 concentration and color coded according to increasing YO-PRO density across the wells according to the dose related sequence blue (live cells), cyan, magenta and green, and this color coding is extrapolated into the following scattergrams, (a2) cell cycle for total DNA versus DNA condensation using Hoechst 33342 (blue channel), (a3) YO-PRO-1 uptake (green integral) versus total DNA (Hoechst 33342 blue integral) or (a4) YO-PRO-1 and PI (orange integral due to the combined color of YO-PRO-1 and PI giving orange) versus total DNA Hoechst 33342 (blue integral); (**b**) Selected individual wells are analyzed for YO-PRO-1 uptake (green integral) versus Hoechst 33342 DNA content (blue integral) ; (**c**) Galleries of specific regions (R2, 3, and 5) of interest determined from the scattergrams, with these regions representing cells that have taken up YO-PRO-1, but in R5 the cells are a still large in size, R3 contain cells which are smaller in size and R2 has the smallest cells as indicated by the boxes on representative cells.

### Mitochondrial Membrane Potential

In the apoptotic drama the mitochondria is a major thespian. Indeed, apoptosis can be divided into extrinsically triggered apoptosis i.e. death receptor-mediated, or intrinsically triggered i.e., involving organelles such as the mitochondria and the ER. Both pathways are able to converge on each other to function as a signaling amplification network to achieve the necessary activation threshold level. The key factors underpinning the instigation of mitochondria apoptosis is the disruption of; (1) mitochondria respiration/metabolism, (2) cellular reduction-oxidation (redox) potential pathway and (3) pro-apoptotic and anti-apoptotic proteins. In many cases the transmembrane potential of the mitochondria drops as a result of the opening of the mitochondrial permeability transition pore, disrupting the $H^+$ gradient across the inner membrane and the respiratory chain, leading to mitochondrial swelling and rupture. Using the Mitoshift Mitochondrial Potential Assay (Trevigen) that employs a cationic probe for gauging mitochondrial membrane potential changes, we evaluated the effect of drug exposure on cells on the mitochondrial membrane potential on the LSC platform. Indeed, the mitochondrial potential sensitive probe was taken up by the mitochondria and upon treatment with MPO-Na a substantial drop in fluorescence, indicative of a decrease in transmembrane potential, was observed (Fig. 3a). Furthermore, KS D-value in Figure 3b showed a significant change in the mitochondria potential with increasing concentration of the compound. The mitochondrial morphology was also analyzed using the LSC's confocal platform, which showed that cells became rounder and smaller and the bright diffused

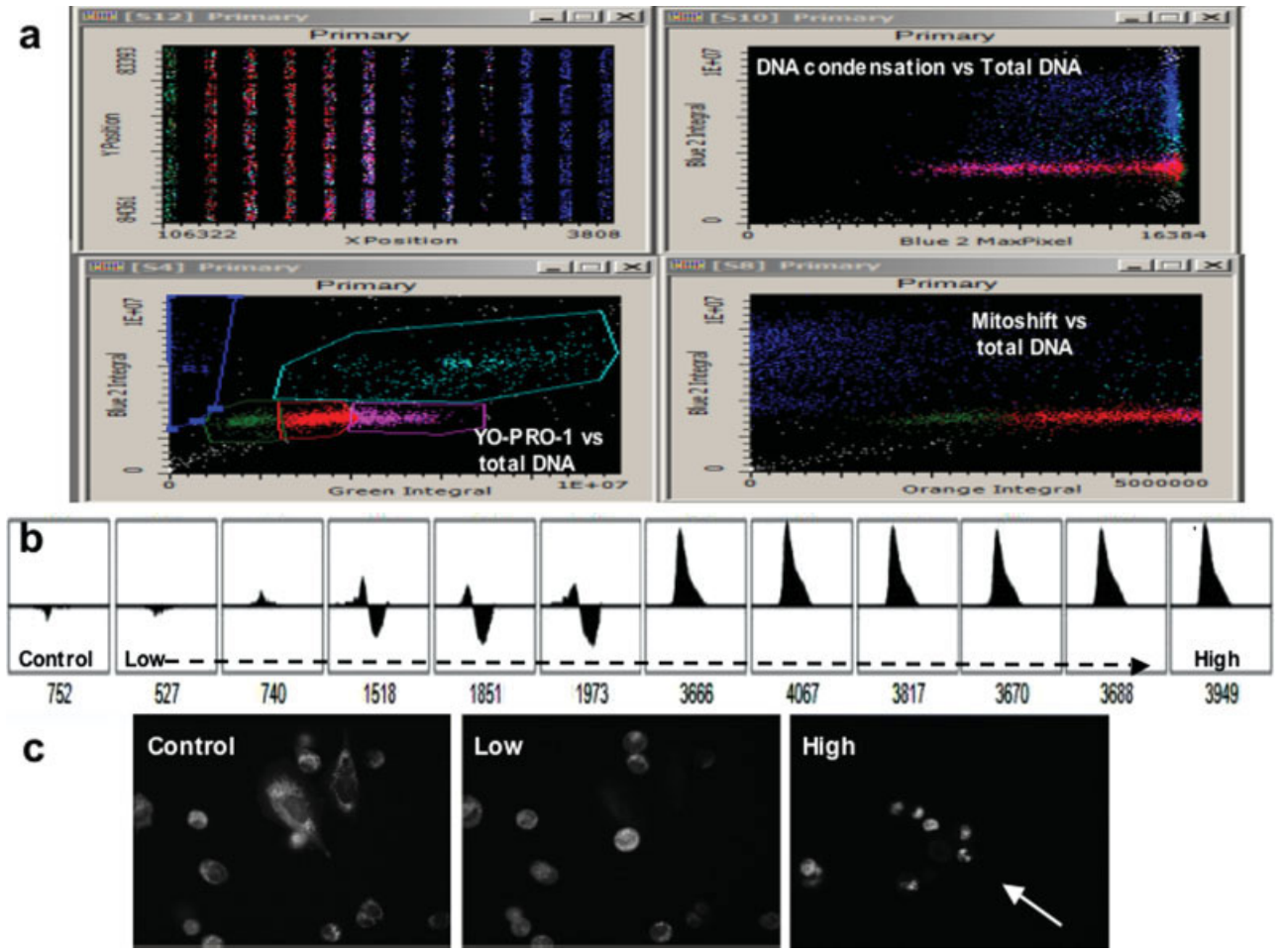


FIG. 3. Cartesian Row Map of Cells Stained with Mitoshift, YO-PRO-1 and Hoechst 33342. Cells were treated with the titrated drug range for 24 h before being stained with Hoechst 33342 (10 μg/ml), Mitoshift (0.1 μg/ml), YO-PRO-1 (10 μg/ml), at 37°C for 30 min. (**a**) YO-PRO-1 (green integral) versus total DNA (blue integral) is plotted as a scattergram, which allows regions (color coded) to be drawn around cell populations based on the DNA content, to distinguish between cells with normal or fragmented nucleus, and the amount of YO-PRO-1 uptake. This color coding is carried into the subsequent scattergram of Mitoshift (orange integral) versus total DNA content (blue integral) as well as the initial row map; (**b**) KS analysis of cells that were treated with the titrated drugs showing the differential effects with regards to the mitochondria potential, with a loss of mitochondria potential as the drug dosage increased; (**c**) Live cell analysis of labeled cells using the confocal ability of the LSC. Cells were labeled with Mitoshift to monitor mitochondrial transmembrane potential. Healthy cells had a diffuse staining in the cytoplasm. The arrows indicate apoptotic cells, which were much smaller in size and exhibited a more concentrated staining pattern with an overall decrease in the number of mitochondria.

staining pattern became more localized with increasing concentration of the drug (Fig. 3c).

## REMARKS AND FUTURE DIRECTIONS

In the 1930s Glucksmann observed three stages of cell death in animal embryos: (1) nuclear precipitation, (2) shrinkage of cytoplasm and nucleus, (3) cellular fragmentation and breakup (27). These observations have stood the test of time, and the future progression in the analysis of apoptosis is concomitant with the development of systems pertaining to multi-parameter analysis of live cells in real time. The development of slide based cytometry, which is extremely versatile in its application range, has been a significant step forward and alleviates some of the issues related to FCM-based analyses. This is not to say that FCM does not serve the general purpose of providing useful information on cellular events in a very user-friendly manner. However, the potential advantage of using a platform such as the LSC lies in its ability to provide a composite analysis of multiple events as they transpire in real-time. Not only are the gross morphological features addressed, but so too are the biochemical changes within a cell, downstream of a stimulus-in this case the use of an apoptosis inducing agent to track the various changes associated with cell death. And all this multi-parameter analysis is possible on the same population of cells or a single cell within a heterogeneous population. We assessed a few classical parameters associated with apoptotic death in a 96-well format, such as plasma membrane permeability changes, DNA integrity and hypo-diploidy, chromatin condensation, loss of mitochondrial membrane potential, and cell cycle profile. These analyses are a sampling of what the LSC platform offers in terms of evaluating multiple variables in one shot.

Future developments will include a long list of biochemical assays, such as kinase activities, protease activities using fluorescence resonance energy transfer (FRET), reactive oxygen species measurement using specific probes, measurement of intracellular glutathione content (reduced vs. oxidized), cytosolic pH measurement [a report by Khoo et al. (28) in the same issue], and assessment of protein-protein interaction, to name a few.

## ACKNOWLEDGMENTS

The authors acknowledge the technical support provide by CompuCyte Corporation,12 Emily Street, Cambridge, MA 02139, USA in running these assays.

## LITERATURE CITED

1. Zamai L, Falcieri E, Zauli G, Cataldi A, Vitale M. Optimal detection of apoptosis by flow cytometry depends on cell morphology. Cytometry 1993;14:891–897.
2. Darzynkiewicz Z, Traganos F. Measurement of apoptosis. Adv Biochem Eng Biotechnol 1998;62:33–73.
3. Kravtsov VD, Daniel TO, Koury MJ. Comparative analysis of different methodological approaches to the in vitro study of drug-induced apoptosis. Am J Pathol 1999;155:1327–1339.
4. Bacso Z, Eliason JF. Measurement of DNA damage associated with apoptosis by laser scanning cytometry. Cytometry 2001;45:180–186.
5. Bacso Z, Everson RB, Eliason JF. The DNA of annexin V-binding apoptotic cells is highly fragmented. Cancer Res 2000;60:4623–4628.
6. Wu X, Simone J, Hewgill D, Siegel R, Lipsky PE, He L. Measurement of two caspase activities simultaneously in living cells by a novel dual FRET fluorescent indicator probe. Cytometry A 2006;69:477–486.
7. Lugli E, Troiano L, Ferraresi R, Roat E, Prada N, Nasi M, Pinti M, Cooper EL, Cossarizza A. Characterization of cells with different mitochondrial membrane potential during apoptosis. Cytometry A 2005; 68:28–35.
8. Diaz D, Prieto A, Barcenilla H, Monserrat J, Sanchez MA, Reyes E, Hernandez-Fuentes MP, de la Hera A, Orfao A, Alvarez-Mon M. Accurate apoptosis measurement requires quantification of loss of expression of surface antigens and cell fragmentation. Cytometry A 2006;69:240–248.
9. Bedner E, Li X, Gorczyca W, Melamed MR, Darzynkiewicz Z. Analysis of apoptosis by laser scanning cytometry. Cytometry 1999;35:181–195.
10. Darzynkiewicz Z, Bedner E, Smolewski P. Flow cytometry in analysis of cell cycle and apoptosis. Semin Hematol 2001;38:179–193.
11. Tarnok A. Slide-based cytometry for cytomics—A minireview. Cytometry A 2006;69:555–562.
12. Kerr JF, Wyllie AH, Currie AR. Apoptosis: A basic biological phenomenon with wide-ranging implications in tissue kinetics. Br J Cancer 1972;26:239–257.
13. Sun Y, Orrenius S, Pervaiz S, Fadeel B. Plasma membrane sequestration of apoptotic protease-activating factor-1 in human B-lymphoma cells: A novel mechanism of chemoresistance. Blood 2005;105:4070–4077.
14. Ahmad KA, Clement MV, Hanif IM, Pervaiz S. Resveratrol inhibits drug-induced apoptosis in human leukemia cells by creating an intracellular milieu nonpermissive for death execution. Cancer Res 2004; 64:1452–1459.
15. Hirpara JL, Seyed MA, Loh KW, Dong H, Kini RM, Pervaiz S. Induction of mitochondrial permeability transition and cytochrome C release in the absence of caspase activation is insufficient for effective apoptosis in human leukemia cells. Blood 2000;95:1773–1780.
16. Campos CB, Paim BA, Cosso RG, Castilho RF, Rottenberg H, Vercesi AE. Method for monitoring of mitochondrial cytochrome c release during cell death: Immunodetection of cytochrome C by flow cytometry after selective permeabilization of the plasma membrane. Cytometry A 2006;69:515–523.
17. Huang X, Kurose A, Tanaka T, Traganos F, Dai W, Darzynkiewicz Z. Sequential phosphorylation of Ser-10 on histone H3 and ser-139 on histone H2AX and ATM activation during premature chromosome condensation: Relationship to cell-cycle phase and apoptosis. Cytometry A 2006;69:222–229.
18. Furuya T, Kamada T, Murakami T, Kurose A, Sasaki K. Laser scanning cytometry allows detection of cell death with morphological features of apoptosis in cells stained with PI. Cytometry 1997;29: 173–177.
19. Kurose A, Tanaka T, Huang X, Traganos F, Dai W, Darzynkiewicz Z. Effects of hydroxyurea and aphidicolin on phosphorylation of ataxia telangiectasia mutated on Ser 1981 and histone H2AX on Ser 139 in relation to cell cycle phase and induction of apoptosis. Cytometry A 2006;69:212–221.
20. Darzynkiewicz Z, Bruno S, Del Bino G, Gorczyca W, Hotz MA, Lassota P, Traganos F. Features of apoptotic cells measured by flow cytometry. Cytometry 1992;13:795–808.
21. Kurose A, Tanaka T, Huang X, Halicka HD, Traganos F, Dai W, Darzynkiewicz Z. Assessment of ATM phosphorylation on Ser-1981 induced by DNA topoisomerase I and II inhibitors in relation to Ser-139-histone H2AX phosphorylation, cell cycle phase, and apoptosis. Cytometry A 2005;68:1–9.
22. Coleman ML, Sahai EA, Yeo M, Bosch M, Dewar A, Olson MF. Membrane blebbing during apoptosis results from caspase-mediated activation of ROCK I. Nat Cell Biol 2001;3:339–345.
23. Bonanno E, Ruzittu M, Carla EC, Montinari MR, Pagliara P, Dini L. Cell shape and organelle modification in apoptotic U937 cells. Eur J Histochem 2000;44:237–246.
24. Messam CA, Pittman RN. Asynchrony and commitment to die during apoptosis. Exp Cell Res 1998;238:389–398.
25. Glisic-Milosavljevic S, Waukau J, Jana S, Jailwala P, Rovensky J, Ghosh S. Comparison of apoptosis and mortality measurements in peripheral blood mononuclear cells (PBMCs) using multiple methods. Cell Prolif 2005;38:301–311.
26. Idziorek T, Estaquier J, De Bels F, Ameisen JC. YOPRO-1 permits cytofluorometric analysis of programmed cell death (apoptosis) without interfering with cell viability. J Immunol Methods 1995;185:249–258.
27. Hamburger V. History of the discovery of neuronal death in embryos. J Neurobiol 1992;23:1116–1123.
28. Koo MK, Chia HO, Holme AL, Pervaiz S. Simultaneous analysis of steady-state intracellular pH and cell morphology by automated laser scanning cytometry. Cytometry A, in press; doi://10.1002/cyto.a. 20361.